DRAFT VERSION MAY 9, 2016
Preprint typeset using LaTeX style emulateapj v. 04/17/13

THE VULTURE SURVEY: ANALYZING THE EVOLUTION OF MGII ABSORBERS

NIGEL L. MATHES[1], CHRISTOPHER W. CHURCHILL[1], AND MICHAEL T. MURPHY[2]

Draft version May 9, 2016

ABSTRACT

We present a detailed measurement of the comoving line density of MgII absorbers as measured in archival VLT/UVES and Keck/HIRES spectra. This survey examines 432 VLT/UVES spectra from the UVES SQUAD collaboration and 170 Keck/HIRES spectra from the KODIAQ group, allowing for detections of intervening MgII absorbers spanning redshifts $0.1 < z < 2.6$. We employ an accurate, automated approach to line detection which consistently detects absorption lines with equivalent widths $W_r < 0.02$ Å in high signal-to-noise spectra. We measure the equivalent widths, apparent optical depth column densities, and velocity widths for each absorbing system. This results in a complete sample of all detectable Mg II absorbers, allowing for accurate determination of the line density of these absorbers across cosmic time. We measure evolution in the number of Mg II absorbers per comoving absorption path, dN/dX, finding more absorbers at $z = 2$ than at present, and signifcantly more high equivalent width absorbers at $z = 2$. We also measure evolution in the equivalent width and column density distributions, parameterized by a Schechter Function fit, finding a shallower weak end slope owing to a relative increase in the number of strong Mg II absorbers around $z = 2$. Finally, we find an three-fold increase in the cosmic mass density of Mg II absorbing systems from $z = 0.1$ to $z = 2.5$. We interpret these findings as the result of the increase in cosmic star formation around $z = 2$ creating and transporting more metal absorbing gas into the halos of galaxies.

Keywords: galaxies: halos — quasars: absorption lines

1. INTRODUCTION

One of the most important questions in modern studies of galactic evolution asks, how do baryons cycle into and out of galaxies, and how does this cycle determine the growth and evolution of galaxies themselves? More specifically, how does the process of gas accretion, star formation, and subsequent supernovae driven feedback shape both the galaxy itself and the circumgalactic medium (CGM) surrounding the galaxy? By using spectroscopic observations of quasars, we can identify and analyze metal line absorbers in and around the halos of foreground galaxies.

Perhaps one of the most prolific absorption featues, the Mg II $\lambda\lambda 2796, 2803$ doublet, traces cool ($T \simeq 10^4$ K) metal enriched gas in the disks and halos of galaxies. It is one of the best tracers of this gas because it can exist in a wide range of ionizing conditions, it is observable in optical wavelengths from redshift $0.1 < z < 2.6$, and it has predictable line characteristics defined by its resonant doublet nature which make it ideal for automated searches.

Many surveys have been undertaken to inventory the cosmic nature of intervening Mg II absorbers. The earliest of those (Lanzetta et al. 1987; Tytler et al. 1987; Sargent et al. 1988; Steidel & Sargent 1992) found that Mg II systems with rest equivalent widths above 0.3 Å show show now evolution in dN/dZ between redshifts $0.2 < z < 2.15$, with dN/dZ increasing slowly with redshift. These studies also found that the equivalent width distribution function, $f(w)$, could be fit equally well with either an exponential or a power law, leaving to question whether the cosmic distribution of Mg II in galactic halos exhibited a fractal, self-similar nature, or if there was a physical limit to size scale and quantity of Mg II absorbing gas.

More modern surveys have taken one of two different approaches to try to analyze the global distribution of Mg II absorbing gas across cosmic time. Churchill et al. (1999) and Narayanan et al. (2007) aimed to analyze the behavior of weak ($W_r(2796) < 0.3$ Å) Mg II absorbers. They find that dN/dZ rises smoothly from $0 < z < 1.4$, but then decreases rapidly around $z \simeq 2$. In addition, the equivalent width distribution function for weak absorbers is best fit by a power law, strongly disfavoring an exponential fit. The implication here is that these weak absorbers, tracing smaller, less kinematically spread Mg II systems, exhibit self-similar behavior in the halos of galaxies and potentially evolve away relative to stronger Mg II absorbing systems at redshifts near the cosmic SFR peak.

The most modern studies employ new multi-object spectrographs such as the Sloan Digital Sky Survey (SDSS) and the FIRE spectrograph on the Magellan Baade Telescope (Nestor et al. 2005; Matejek & Simcoe 2012). These surveys aim to use massive quantities of quasar spectra in order to remove uncertainties in the distribution of strong intervening absorbers. Nestor et al. (2005), examining over 1300 Mg II absorbers with $W_r(2796) > 0.3$ Å, find that the equivalent width distribution function is well fit by an exponential. They do not find evidence for redshift evolution in systems with $0.4 < W_r(2796) < 2$ Å, but see a decrease in the number of lines stronger than $W_r(2796) > 2$ Å as redshift decreases, towards $z < 1$. Matejek & Simcoe (2012), looking at 111 Mg II absorbing systems from $1.9 < z < 6.3$, also find that the equivalent width distribution function is well fit by an exponential. They do note, however, that $f(W)$ steepens at redshifts below $z = 3$, implying some causal connection between the $f(W)$ and the cosmic SFR peak. They also observe that systems with $W_r(2796) < 1.0$ Å show no evolution with redshift, but stronger systems increase nearly three-fold in dN/dZ from low redshift to $z \simeq 3$.

For our survey, we aim to analyze largest, most compre-

[1] New Mexico State University, Las Cruces, NM 88003
[2] Swinburne University of Technology, Victoria 3122, Australia

hensive sample of high resolution, high signal-to-noise quasar spectra to uniformly observe both strong and weak Mg II absorbers. We hope to finally rectify the discontinuities in prior Mg II absorption line surveys by analyzing large numbers of both strong and weak absorbers. To do so, we will examine 602 quasar spectra spanning emission redshifts from $z = 0.014$ to $z = 5.292$ observed with either the VLT/UVES or KECK/HIRES spectrographs. We detect over 1200 Mg II absorbing systems from $0.14 < z < 2.63$ to a detection limit of $W_r(2796) \simeq 0.02$. We aim to characterize the evolution in the number density of all Mg II absorbers from present to beyond the peak of the cosmic star formation rate.

We begin by explaining the methods of acquiring and analyzing the quasar spectra in section 2. Next, in section 3, we present the results showing the evolution of the Mg II equivalent width distribution, dN/dX, and the Mg II column density distribution across redshift. In section 4 we analyze the funcitonal fit to the column density distribution and derive the relative matter density contributed to the universe by Mg II, $\Omega_{\rm Mg\,II}$. In Section 5 we summarize our results and look to future studies using this rich data set, including a companion analysis of intervening C IV absorbers and detailed kinematic analysis of intervening absorbing systems. For all calculations, we adopt the most recently published Planck cosmology, with $H_0 = 67.74\,{\rm kms^{-1}Mpc}$, $\Omega_M = 0.258$, and $\Omega_\Lambda = 0.742$.

2. DATA AND ANALYSIS

2.1. *Quasar Spectra Sample*

We have assembled a sample of 602 archival quasar spectra observed with the VLT/UVES and KECK/HIRES spectrographs. The data originate from two archival data mining efforts - the UVES Squad collaboration (432 spectra) led by Michael Murphy, and the KODIAQ Survey (170 spectra) led by John O'Meara (O'Meara et al. 2015). The spectra range in signal-to-noise from XXX to YYY, quasar emission redshifts span $XXX < z < YYY$, and wavelength coverage for each spectrum spans either $3000-6600$ or $3000-10,000$, depending upon whether the red arm of each spectrograph was used.

2.2. *Continuum Fitting and Line Detection*

The KODIAQ data sample is reduced and fully continuum fit, delivered as normalized spectra according to the prescriptions of O'Meara et al. (2015). The UVES Squad sample also comes reduced, but with an automatic, low order polynomial continuum fit applied. This fit can incorrectly estimate the continuum around narrow emission regions and broad absorption features. For the UVES data sample, I add a higher order continuum fit to difficult regions of the spectra. We use UVES_popler, an ESO/VLT UVES post-pipeline echelle reduction program written by Michael T. Murphy (Copyright 2003-2015 Michael T. Murphy) to apply these fits, preserving continuity of the continuum with non-absorbing regions.

The next step involves detecting all Mg II absorption features. We first limit the search range to regions of the spectrum redward of the Ly α emission, as Ly α forest contamination would render automatic detection of weaker metal lines nearly impossible. We also do not search 5000 km s^{-1} blueward of the quasar emission redshift in order to avoid absorbers associated with the quasar itself. Finally, we exclude regions of strong telluric absorption bands, specifically from $6277-6318$, $6868-6932$, $7594-7700$, and $9300-9630$, finding that the molecular line separations and ratios can lead to numerous false positives when searching for Mg II doublets.

To find all intervening Mg II $\lambda\lambda 2796, 2803$ absorbers, we employ a techinque outlined in Zhu & Ménard (2013), in which we perform a matched filter search for absorption candidates detected above a certain signal-to-noise (S/N) threshold. The filter is a top hat function centered at the wavelength of the desired redshifted absorption line. Its width is selected to match the resolution of the spectrograph used (VLT/UVES $\simeq$ 40,000; KECK/HIRES $\simeq$ 45,000), set as the FWHM of an unresolved gaussian absorption feature. We convolve the filter with the normalized spectrum to generate a normalized power spectrum in redshift space, with absorption features having positive power.

Because the error spectrum in both instruments is complicated and often discontinuous, we cannot convolve the filter with the error spectrum to derive normalized noise estimates, as is often done in matched filter analysis. Instead, we examine the noise in the derived power spectrum. We sigma clip chunks of the power spectrum before calculating its standard deviation. We take the standard deviation as the normalized noise and use it to calculate the signal-to-noise of the absorption features in the power spectrum as the ratio of the normalized power (S) to the normalized noise (N). A flagged absorption feature has $S/N > 5$. A confirmed doublet detetection for Mg II $\lambda\lambda 2796, 2803$ requires detection of $S/N_{2796} > 5$ and $S/N_{2803} > 3$. In addition, in our automated routines we remove detections with non-physical doublet ratios in unsaturated regions; specifically, we exclude cases where $W_r(2803) > W_r(2796)$ and $W_r(2803) < 0.3 \times W_r(2796)$. We relax this constraint in saturated lines.

All absorption features are visually verified upon completion of the detection algorithm. Multiple feature detections within ± 500 km s^{-1} of each other are grouped together to generate absorption systems to be analyzed. Once absorption systems are identified, we calculate the optical depth-weighed median absorption redshift to define the center of the entire absorption system. The formal derivation of this redshift is described in the appendix of Churchill & Vogt (2001).

We also derive an equivalent width detection limit across the spectrum. To do so, we model gaussian features across the spectrum and assume a full-width at half-max (FWHM) defined by the resolution of the instrument to represent unresolved lines. The height of the gaussian is then calculated as the height at which the modelled line would be detected using our matched filterting technique with a $S/N = 5$. We then integrate to find the equivalent width, and take that value as the minimum detectable equivalent width at a given wavelength. This full equivalent width detection limit spectrum will allow us to accurately characterize the completeness of our sample, along with the full redshift path length searched.

2.3. *Measuring Absorption Properties*

For each absorption system, we automatically define the wavelength bounds of each absorbing region by finding where 3 pixels of the absorption trough recover past the 1σ error level in the spectrum. Within these regions we calculate equivalent widths (W_r), velocity widths (Δv), kinematic spreads (ω_v), apparent optical depth (AOD) column densities ($log(N)$), and absorption asymmetries. The functional forms of these parameters are detailed in the appendicies of Churchill & Vogt (2001), equations A3 – A7.

3. RESULTS

3.1. *Sample Characterization*

Figure 1 shows the relationships between the measured absorption parameters, characterizing the distribution of absorption properties for our survey. With redshift, there are no obvious trends other than the highest equivalent width absorbers, with $W_r^{2796} > 4$, existing at $z > 1.5$. The data gaps at $z = 1.7$ and $z = 2.4$ represent the omitted search regions which overlap with the stronger telluric absorption bands. With column density, we see the normal trends of higher column density systems exhibiting higher equivalent widths and velocity spreads, with the distributions asymptoting near $\log N \simeq 15$ due to saturation effects and the nature of measuring column densities with the AOD method. With respect to kinematic spread, we observe the sharp cutoff in the ω_v vs. W_r^{2796} relationship because of W_r^{2796}'s dependence upon velocity width.

3.2. *Sample Completeness and Survey Path Coverage*

Figure 2 shows the function $g(W_r^{2796}, z)$. This 2D heat map details the number of spectra in which a Mg II $\lambda\lambda 2796, 2803$ doublet could be detected as a function of the equivalent width detection limit and redshift. The vertical stripes with no redshift path coverage represent the omitted telluric absorption regions for our survey. The integral along a given W_r^{2796} slice gives the total redshift path length available for the sample.

3.3. *dN/dZ and dN/dX*

Previous studies of the statistical properties of Mg II absorbers have been forced to focus either on strong or weak absorbers. The largest sample of quasar spectra originates from the Sloan Digital Sky Survey (SDSS), which employs a spectrograph with an instrumental resolution around 69 km s^{-1}, limiting SDSS absorption surveys to strong absorbers (Zhu & Ménard 2013; Cooksey et al. 2013) (MORE CITATIONS). Conversely, previous studies of weak absorbers used small samples of quasar spectra, never exceeding 50 quasar spectra (Kacprzak et al. 2011) (MORE CITATIONS). In this paper, we aim to characterize the evolution of the incidence rate, number density per absorption path length, and cosmic mass density of all Mg II absorbers above a detection limit of $W_r(2796) > 0.02$ Å from redshifts $0.18 < z < 2.57$.

The number density of Mg II absorbers per redshift path length and its associated variance is defined as

$$\frac{dN}{dZ} = \sum_i \frac{1}{\Delta Z(W_r^i)}, \quad \sigma^2_{\frac{dN}{dZ}} = \sum_i \left[\frac{1}{\Delta Z(W_r^i)}\right]^2, \qquad (1)$$

where we count the number of Mg II absorbers, dividing by the total searched redshift path length (ΔZ), defined as

$$\Delta Z(W_r^i) = \int_{z_1}^{z_2} g(W_r^i, z)\, dz, \qquad (2)$$

where $g(W_r, z)$ is the equivalent width sensitivity function. Equation (6) in Lanzetta et al. (1987) defines $g(W_r, z)$, which counts the number of spectra in which a given equivalent width absorption feature may be detectected at the 5σ level in a given redshift interval.

The comoving Mg II absorber line density and its associated variance is defined as

$$\frac{dN}{dX} = \sum_i \frac{1}{\Delta X(W_r^i)}, \quad \sigma^2_{\frac{dN}{dZ}} = \sum_i \left[\frac{1}{\Delta X(W_r^i)}\right]^2, \qquad (3)$$

where we count the number of Mg II absorbers, dividing by the total searched absorption path (ΔX), defined as

$$\Delta X(W_r^i) = 2\sqrt{\Omega_M(1+\Delta Z(W_r^i))^3 + \Omega_\Lambda}/(3\Omega_M), \qquad (4)$$

where Ω_M is the cosmic matter density, and Ω_Λ is the cosmic density attributed to dark energy.

In Figure 3, we plot dN/dX as a function of redshift for varying equivalent width cuts. Dotted lines are fit according to the analytical form which allows for redshift evolution in dN/dX, defined as,

$$\frac{dN}{dX} = n\sigma(1+z)^\epsilon, \qquad (5)$$

where n is the number density of Mg II absorbers, σ is the absorbing cross-section, and ϵ is the power dependence of dN/dX on redshift. We find that the best-fit value of ϵ increases with increasing equivalent width cuts, with the distribution showing a steeper dependence on redshift as we observe larger and more complex Mg II absorbing systems. This trend is driven primarily by an enhancement in dN/dX for the strongest Mg II absorbers around $z = 2$, relative to lower redshifts. We suspect that the correlation between this enhancement and the cosmic SFR peak is not coincidence, and that these stronger Mg II absorption systems are direct byproducts of star formation driven winds in this same epoch.

3.4. *Equivalent Width Frequency Distribution*

To calculate the equivalent width frequency distribution, we calculate dN/dX for each absorber equivalent width, sum the distribution in equivalent width bins, and then divide by the bin width. We divide the sample into four redshift regimes, ensuring that the number of absorbers in each redshift chunk remains constant. The result is a characteristic number density of Mg II absorbers per absorption path length as a function of their equivalent width.

In Figure 4, we plot the equivalent width frequency distribution. We fit this distribution with a Shechter function to parameterize the distribution and to compare the relative differences between varying redshift cuts. We find the low equivalent width slope decreases towards shallower values as redshift increases, implying a decrease in weak Mg II absorbers and a relative increase in strong Mg II absorbers from low redshift to redshifts near $z = 2$.

3.5. *Column Density Distribution*

To calculate the column density distribution, we calculate dN/dX for each absorber equivalent width, sum the distribution in column density bins, and then divide by the bin width. The result is a characteristic number density of Mg II absorbers per absorption path length as a function of their column densities. It should be noted that at high column densities near $\log(N(MgII)) = 15$, the measured column densities are lower limits as the AOD method to measure column densities cannot constrain the true column when the line saturates.

In Figure 5, we plot the column density frequency distribution. Again, we fit this distribution with a Schechter function. We find again that the low column density end of the distribution becomes shallower as one goes from low redshift to $z = 2$. Due to saturation effects, the final high column density bin is likely best regarded as a lower limit.

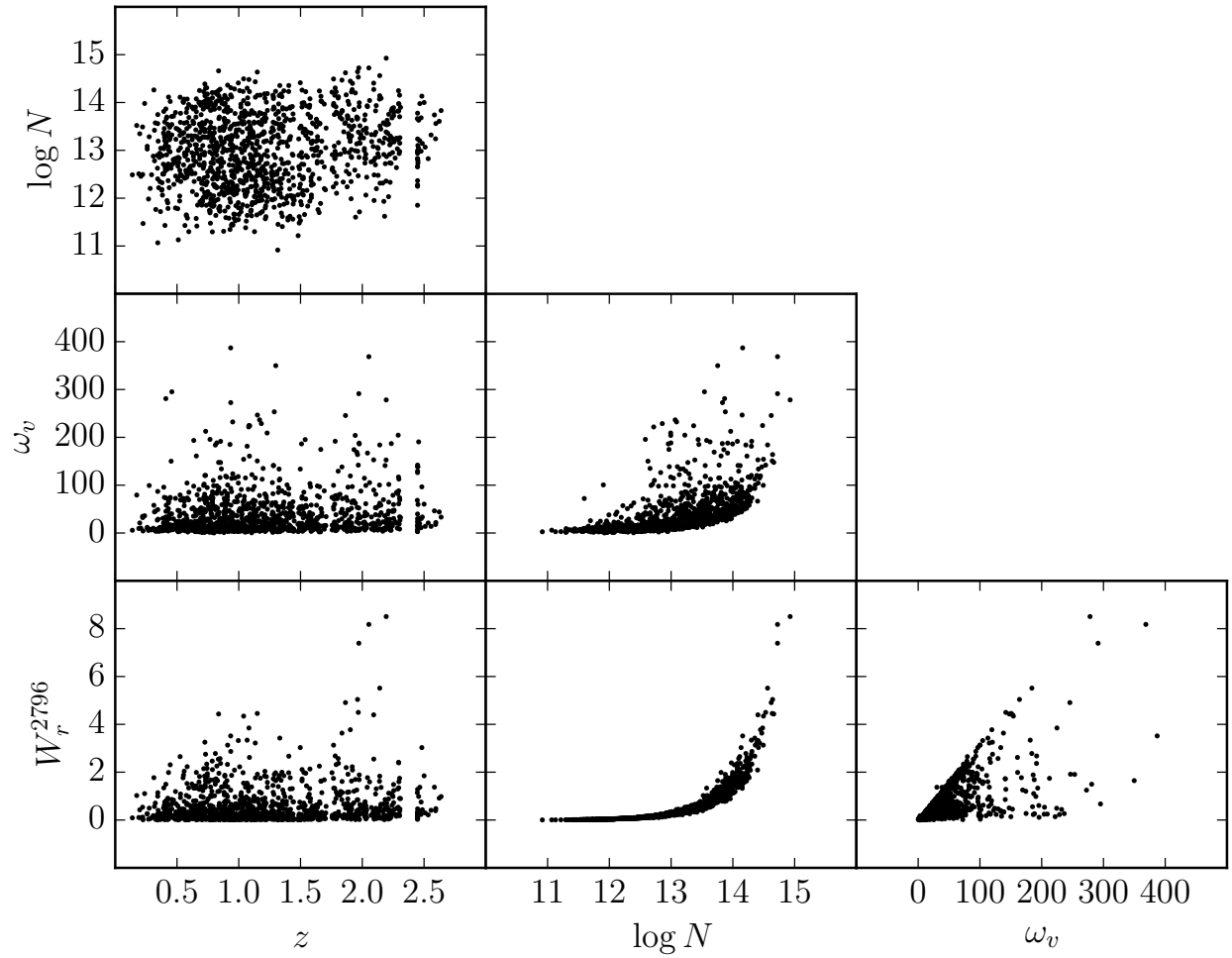

Figure 1. Correlations between measured absorption properties for survey sample. $\log N$ is the AOD column density, ω_v is the kinematic spread, W_r^{2796} is the rest frame Mg II2796 equivalent width, and z is the absorption redshift.

4. DISCUSSION

4.1. *Evolution of MgII Distributions*

Narayanan et al. (2007) measure the evolution of weak Mg II absorbers from $0.4 < z < 2.4$ in VLT/UVES spectra. They compare to Churchill et al. (1999), which fits the equivalent width distribution with a power law, and to Nestor et al. (2005), which fits an exponential to $f(W_r)$. In the case of weak absorbers at $z < 1.4$, Narayanan et al. (2007) finds that a power law with a slope of $\alpha = -1.04$ is a satisfactory fit, mirroring the results from Churchill et al. (1999). However, when examining the higher redshift half of their sample, they find a decreased number of weak Mg II absorbers and prefer the exponential fits of Nestor et al. (2005). Unfortunately, they do not also entertain the thought that a shallower power law slope, such as $\alpha = -0.8$, also accurately characterizes the equivalent width distribution of weak Mg II absorbers.

Narayanan et al. (2007) also analyze the evolution of dN/dZ with redshift for weak Mg II absorbers. They find that the distribution follows the classical "no evolution" assumption; that is, the expected number density for a nonevolving population of absorbers in a ΛCDM universe, at redshifts less than $z = 1.5$. At higher redshift, they find the number density of weak absorbers decreases. Here, in our study, we find similar behavior for absorbers with $0.02 \leq W_r(2796) < 0.3$ Å, except we observe the relative decrease in dN/dZ occurring around $z = 1$.

Steidel & Sargent (1992), and later Churchill & Vogt (2001), examine the redshift evolution of dN/dZ for strong Mg II absorbers with $W_r(2796) > 0.3$ Å. They find that the number density of strong Mg II absorbers increases from $z = 0$ to $z = 2.2$, however they cannot derive the slope of this trend to sufficient accuracy to distinguish between an evolving population or a non-evolving population. We perform a similar analysis on our sample, calculating instead dN/dX to distill the analysis, as a flat distribution in dN/dX implies no evolution. When we take absorbers with $W_r(2796) > 0.3$ Å, we find that a fit to the function $dN/dX = n(1+z)^{\epsilon}$ with a slope of $\epsilon = 1.62$ is appropriate, implying that the number density of strong Mg II absorbers does indeed evolve, with more strong absorbers appearing around $z = 2$.

Kacprzak & Churchill (2011) combine multiple previous studies to accurately characterize the equivalent width distri-

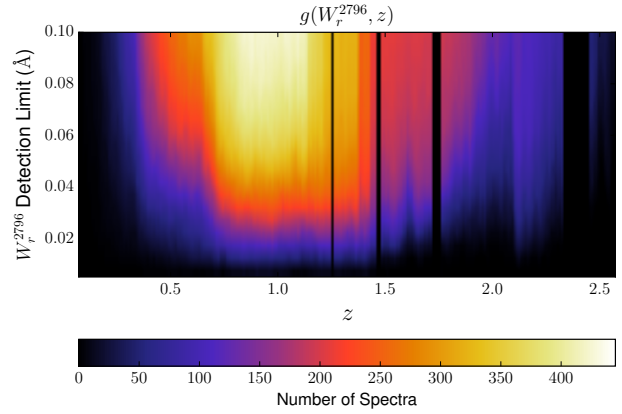

Figure 2. The function $g(W_r^{2796}, z)$ shown as 2D heat map with the colors representing the value of $g(W_r^{2796}, z)$. This is the number of spectra in which an absorption line of a given equivalent width and a given redshift may be detected according to the detection limit of the spectrum. The vertical black bars representing no redshift path length coverage show the omitted wavelength regions of the survey based upon contaminating telluric absorption features.

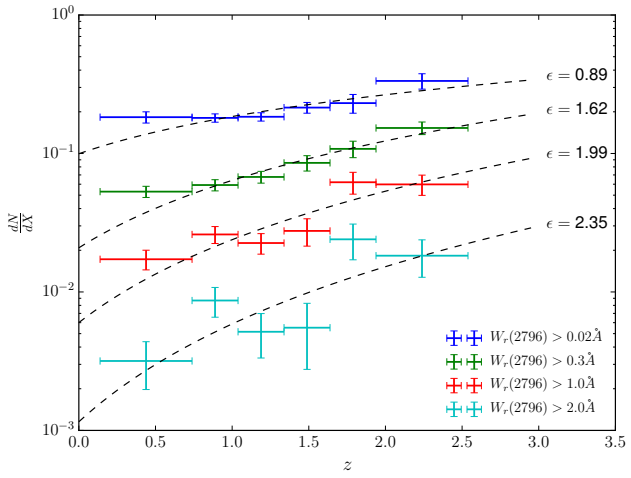

Figure 3. $\frac{dN}{dX}$ as a function of redshift for varying $W_r(2796)$ cuts. Colors represent different equivalent width cuts. The black dotted lines are fits to the distribution of the functional form $f(z) = n\sigma(1+z)^{\epsilon}$, with the best fit ϵ value labelled. We see increasing values of ϵ with increasing equivalent width, driven by an enhancement of stronger Mg II absorbers around redshift 2 compared to lower redshifts.

bution function, $f(W_r)$. They find a Schechter function with a low equivalent width slope of $\alpha = -0.642$ and an exponential cutoff of $W_* = 0.97$ Å best fit the data. Performing the same analysis with our survey, we find a faint end slope of $\alpha = -0.9$ and an exponential cutoff at $W_* = 1.66$ Å. COMPARE AND DISCUSS.

4.2. $\Omega_{\rm Mg\,II}$

We now aim to calculate the matter density of Mg II absorbers across cosmic time. To do so, we employ the following equation,

$$\Omega_{MgII} = \frac{H_0\, m_{Mg}}{c\ \rho_{c,0}} \int_{N_{min}}^{N_{max}} f(N_{MgII}) N_{MgII}\, dN_{MgII}, \qquad (6)$$

where H_0 is the Hubble constant today, $m_{Mg} = 4.035 \times 10^{-23}$ g, c is the speed of light, $\rho_{c,0}$ is the critical density at present, $f(N_{MgII})$ is the column density distribution of MgII absorbers, and N_{MgII} is the column density. Using our derived fit to the column density distribution, we are able to numerically integrate the first moment from $0 < N(MgII) < 20$ cm^{-2}. The results are shown below in Figure 6.

Errors are derived by bootstrap Monte-Carlo. We pick at random with replacement column densities from the sample of measured column densities for all of our Mg II absorbers. We then recalculate the column density distribution, find the best parameterized Schechter fit, and then integrate and compute Equation 6. We take the standard deviation about the mean of this ensemble of simulated measurements as the error in Ω_{MgII}.

4.3. *Potential Causes for Trends*

The most obvious conclusion to be drawn from our Mg II survey is that around redshift $z = 2$, something changes in the distribution of Mg II absorbers. The number of strong absorbers per unit path length increases, the faint end slope of the equivalent width and column density distributions flattens, the 'knee' of the Shechter fit of the equivalent width and column density distributions pushes outward to higher $W_r(2796)$ and N(Mg II), and the cosmic mass density of Mg II increases. We can now confidently state that the physical properties driving the global distribution of Mg II absorbers changes around $z = 2$. Possible explanations relate to the ionization conditions in the halos of galaxies at this time, the metallicity of gas around galaxies, or the quantity of metals in the circumgalactic medium.

Haardt & Madau (2012) represents the most recent and robust estimate of the cosmic ionizing background as a function of redshift, which is the primary ionizing component responsible for the global ionization state of gas in galactic halos. From redshift $z = 1.1$ to redshift $z = 3.0$, the comoving emissivity increases dramatically for photon energies above 3 eV. As the number of ionizing photons in the IGM increases, holding constant the density and quantity of metals in galactic halos, we would nominally expect for the ionization parameter of absorbers in the halos of galaxies to increase. Increasing the ionization parameter should decrease the observed quantity of Mg II seen at $z = 2$ relative to lower redshifts as Mg II favors lower ionization parameter conditions. This is not what we observe in our sample, and we therefore disfavor the hypothesis that changes in ionzation conditions in the halos of galaxies could drive the observed increase in the number of strong Mg II absorbers at redshift $z = 2$.

The metallicity of galaxy halos as a whole is not well characterized over time. However, if we assume that the metals in galaxy halos are built up as a result of outflows (Quiret et al. 2016), and that the metallicty of the halo may scale with the metallicity of the ISM, then it would make no sense to observe larger quantities of Mg II in the circumgalactic medium at $z = 2$ compared to $z < 1$. In fact, under these assumptions, the metals should build up over time in the halos of galaxies, producing stronger Mg II absorption at lower redshift. Cosmic metallicity evolution, then, cannot drive the observed trends.

This leaves us, then, with the most likely conclusion being that galaxies eject more metals into their halos around $z = 2$.

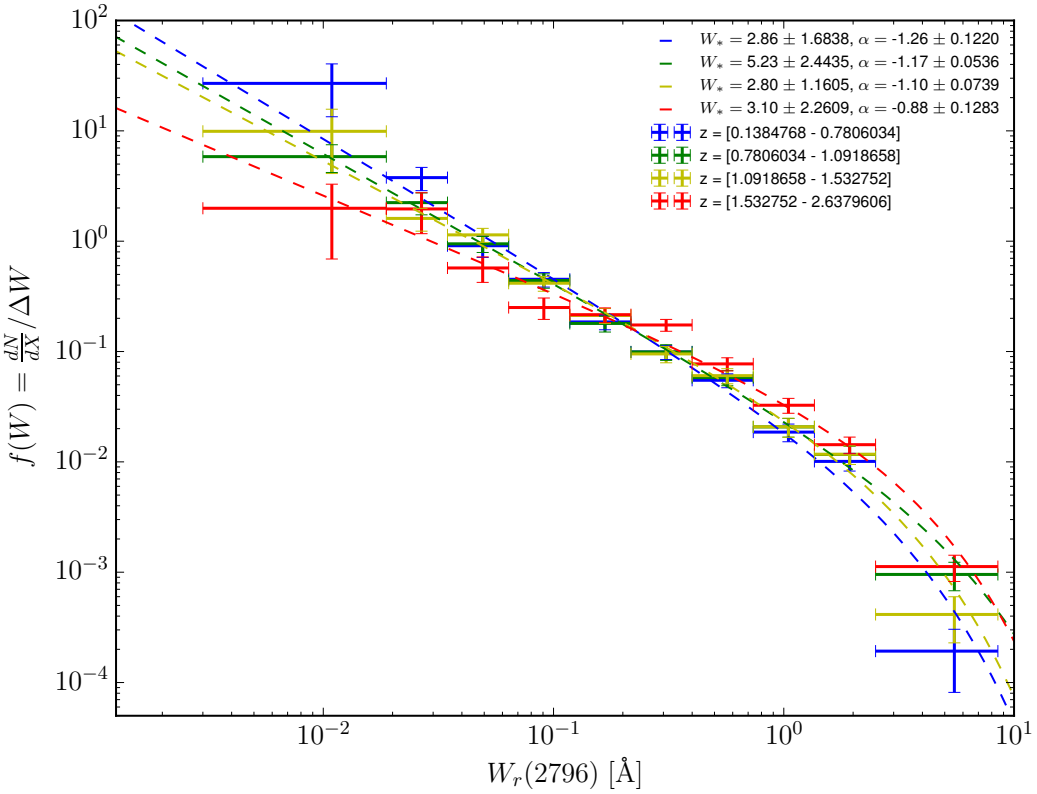

Figure 4. The equivalent width distribution of Mg II absorbers, defined as the comoving line density ($\frac{dN}{dX}$) in each equivalent width bin divided by the bin width. We fit this distribution with a Schechter function, capturing the self-similar power law behavior of the distribution before the exponential cutoff limiting the size of Mg II absorbers.

Behroozi et al. (2013) combines data from 19 independent studies from 2006 – 2012 of the cosmic star formation rate to find that it rises with significant scatter from $z = 8$ to $z = 2$, where it peaks before falling off with a steeper slope towards $z = 0$. Galaxies at $z = 2$ were forming stars at higher rates than any other time in cosmic history. In addition, studies associated with COS-Halos seeking to understand the distribution of metals around galaxies have found the majority of cool, metal absorbing gas lies within the virial radius of galaxies (Peeples et al. 2014). Stern et al. (2016) also find that the mean cool gas density profile around galaxies scales as R^{-1}, with most strong, low ionization metal absorbers existing near the galaxy itself.

Therefore, we now favor a picture where galaxies, undergoing their most rigorous stage of global star formation in cosmic history, expell large quantities of metal enriched gas into their halos through star formation driven outflows at $z = 2$.

5. CONCLUSIONS

Using archival data from *VLT*/UVES and *KECK*/HIRES, we have undertaken the most complete survey of Mg II absorbers in 602 quasar spectra in high resolution (~ 7 km s^{-1}) allowing for the detection of both strong and weak Mg II absorbsers. Our survey spans absorption redshifts from $0.18 < z < 2.57$, allowing for characterization of the evolution of the distribution of these absorbers across cosmic time. Using our own detection and analysis software, we are able to accurately characterize the equivalent width detection limit, absorption path length, and survey copmleteness to a level allowing for an accurate determination of dN/dZ, the equivalent width distribution function, the column density distribution function, and the total cosmic mass density of Mg II absorbers. Our main findings are as follows:

1. We find 1209 isolated Mg II absorption line systems with equivalent widths from 0.003 Å to 8.5 Å, and redshifts from $z = 0.14$ to 2.63.

2. The distribution of the number density of Mg II absorbers, dN/dX, evolves over time, increasing from low redshift to high redshift. In addition, this evolution is more drastic, with an emperical fit to the distribution in the form of $dN/dX = n(1+z)^{\epsilon}$ showing ϵ increasing from $\epsilon = 0.89$ for all absorbers with $W_r(2796) > 0.2$ Å to $\epsilon = 2.35$ for absorbers with $W_r(2796) > 2$ Å.

3. The equivalent width distribution function and the column density distribution function for Mg II absorbers are well fit by a Schecter Function, with a characteristic normalization, faint end slope, and exponential cutoff. Both functions show redshift evolution, specifically in the faint end slope, with this slope becomming shallower for redshifts near $z = 2$. The cause for this decrease in faint end slope is the increase in relative number of high equivalent width, high column density Mg II absorbers at $z = 2$.

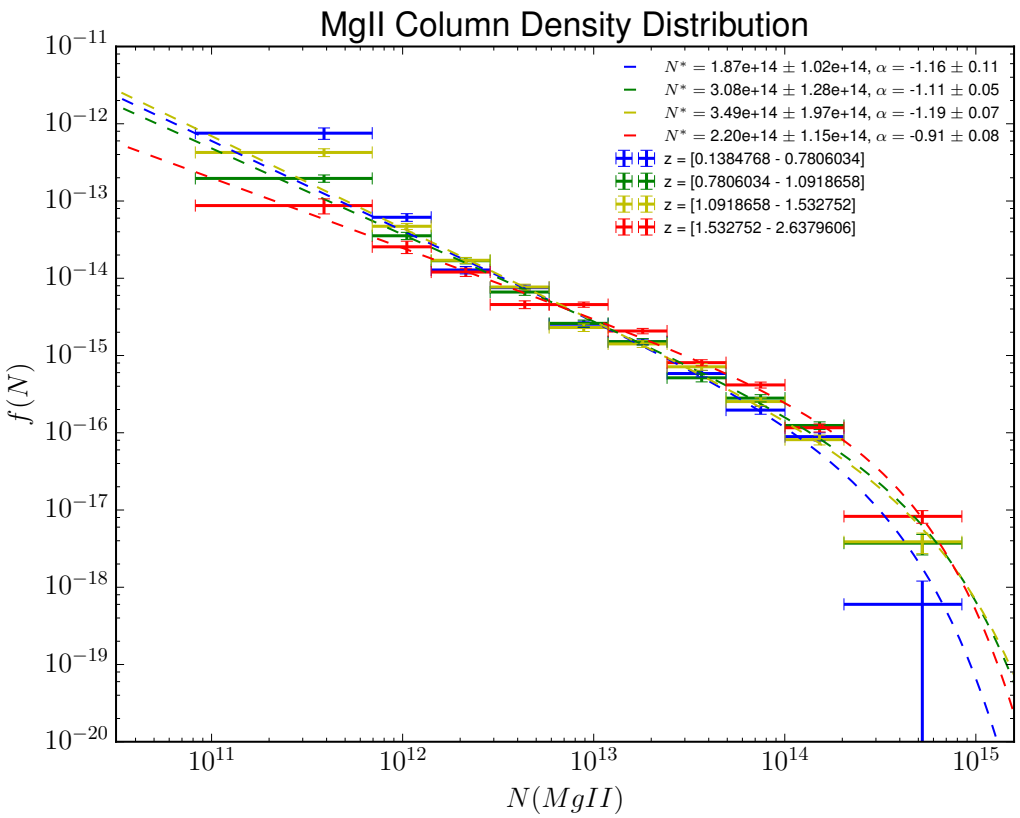

Figure 5. The column density distribution of Mg II absorbers, defined as the comoving line density in each column density bin divided by the bin width. We fit this distribution with a Schechter function.

4. The cosmic mass density of Mg II absorbing gas, $\Omega_{\rm Mg\,II}$, increases from $\Omega_{\rm Mg\,II} \simeq 1 \times 10^{-9}$ at $z = 0$ to $\Omega_{\rm Mg\,II} \simeq 3 \times 10^{-9}$ at $z = 2.5$.

5. We interpret these trends as owing to the increased star formation activity in galaxies at $z = 2$, ruling out other possible drivers such as changes in the ionizing radiation at these times and changes in the metallicity of galactic halo gas. The physical interpretation relies on galaxies creating more metal enriched gas at this time through supernovae driven winds, and expelling it into the circumgalactic medium.

Acknowledgements.

REFERENCES

Behroozi, P. S., Wechsler, R. H., & Conroy, C. 2013, ApJ, 770, 57
Churchill, C. W., Rigby, J. R., Charlton, J. C., & Vogt, S. S. 1999, ApJS, 120, 51
Churchill, C. W., & Vogt, S. S. 2001, AJ, 122, 679
Cooksey, K. L., Kao, M. M., Simcoe, R. A., O'Meara, J. M., & Prochaska, J. X. 2013, ApJ, 763, 37
Haardt, F., & Madau, P. 2012, ApJ, 746, 125
Kacprzak, G. G., & Churchill, C. W. 2011, ApJ, 743, L34
Kacprzak, G. G., Churchill, C. W., Evans, J. L., Murphy, M. T., & Steidel, C. C. 2011, MNRAS, 416, 3118
Lanzetta, K. M., Turnshek, D. A., & Wolfe, A. M. 1987, ApJ, 322, 739
Matejek, M. S., & Simcoe, R. A. 2012, ApJ, 761, 112
Narayanan, A., Misawa, T., Charlton, J. C., & Kim, T.-S. 2007, ApJ, 660, 1093
Nestor, D. B., Turnshek, D. A., & Rao, S. M. 2005, ApJ, 628, 637
O'Meara, J. M., Lehner, N., Howk, J. C., et al. 2015, AJ, 150, 111
Peeples, M. S., Werk, J. K., Tumlinson, J., et al. 2014, ApJ, 786, 54
Quiret, S., Péroux, C., Zafar, T., et al. 2016, MNRAS
Sargent, W. L. W., Steidel, C. C., & Boksenberg, A. 1988, ApJ, 334, 22
Steidel, C. C., & Sargent, W. L. W. 1992, ApJS, 80, 1
Stern, J., Hennawi, J. F., Prochaska, J. X., & Werk, J. K. 2016, ArXiv e-prints
Tytler, D., Boksenberg, A., Sargent, W. L. W., Young, P., & Kunth, D. 1987, ApJS, 64, 667
Zhu, G., & Ménard, B. 2013, ApJ, 770, 130

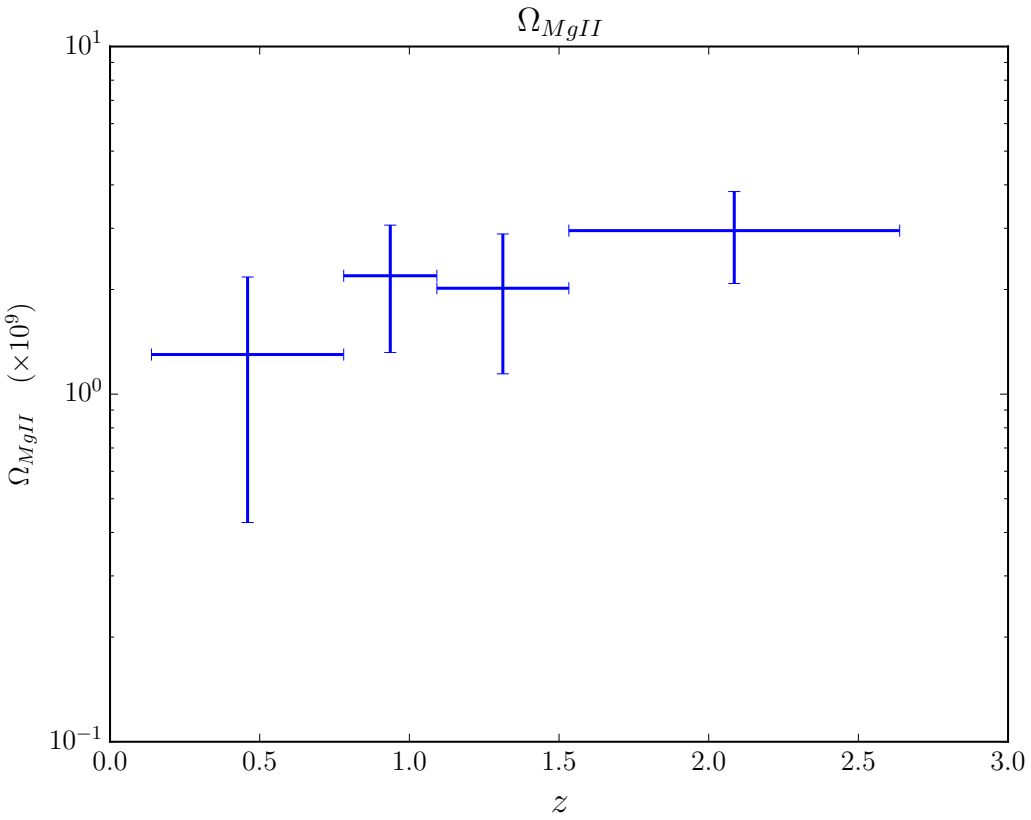

Figure 6. $\Omega_{\mathrm{Mg\,II}}$ as a function of redshift. The cosmic mass density of Mg II stays roughly flat near a value of 1×10^{-9}, with a potential increase from $z = 0.1$ to $z = 2.5$.